Optical Materials 113 (2021) 110887

Contents lists available at ScienceDirect

Optical Materials

journal homepage: http://www.elsevier.com/locate/optmat

Research Article

Effect of Fe_3O_4 in enhancement optical and gamma ray absorption properties of geopolymer apron cassava starch/black carbon/glycerin

Nurlaela Rauf, Zulkifli Tri Darmawan, Sultan Ilyas, Heryanto Heryanto, Ahmad Nurul Fahri, Roni Rahmat, Bualkar Abdullah, Dahlang Tahir *

Department of Physics, Hasanuddin University, Makassar, 90245, Indonesia

ARTICLE INFO

Keywords:
Geopolymer apron
Cassava starch
Fe_3O_4
Carbon black
Tensile strength
XRF
Absorbed dose

ABSTRACT

Geopolymer apron cassava starch/BC/Fe_3O_4/glycerin has been synthesized for various amount of Fe_3O_4 (0.5%, 1%, and 1.5%) into cassava starch and black carbon (BC) solutions. The quantitative analysis from Fourier transforms infra-red (FTIR) was used to determine the optical properties, dielectric function, energy loss function, attenuation constant, and propagation constant. The higher value of the distance between two optical ((LO-TO)) phonon vibration, attenuation constant, propagation constant was strong correlation with higher absorption properties and higher mechanical properties. The effectiveness of radiation shielding also from the density, linear attenuation coefficient (μ), mass attenuation coefficient (μs), half value layer (HVL), and mean free path (MFP) from gamma radiation source IBT 103 Cs 137. The attenuation was 0.178 cm^{-1}, sample density was 0.984 g/cm^3, HVL value was 3.893 cm, and MPF was 5.618 cm. The best characteristic in supporting composite performance as an apron applications are for 1.5% Fe_3O_4 in the composite. This study shows that the FTIR spectra could be useful for determining the optical properties, phonon vibration, dielectric function, energy loss function, attenuation constant, and propagation constant of composite apron cassava starch/BC/Fe_3O_4/glycerin.

1. Introduction

Anti-radiation apron is one of the required protective devices for radiation workers [1,2]. Most of the aprons produced by the industries from the lead plate which are heavy and stiff which makes it uncomfortable for radiation workers [3–5].

The utilization of the aprons for radiation protective devices is needed [4,6]. The NCRP (The US National Council on Radiation Protection and Measurements) provided limits of minimum dose per year is 50 mSv for radiologists and medical staff and 3 mSv for other medical workers such as spine surgeons. While, people who do not work in the radiation field, the limit annually is not exceeding than 1 mSv [7].

Seung-Jae Hyun *et* al in 2016 [7] reported that the lead (Pb) aprons with a thickness of 0.25 and 0.5 mm capable of attenuating about 90% and 99% of the radiation dose, respectively. Pb material is the basic content for the apron filler for protection ionizing radiation. Pb is a heavy, toxic metal, and will trigger environmental damage [6,8]. There are many natural materials that can be used for gamma radiation shielding such as carbon and iron [9]. Iron and iron oxide is used to increase the attenuation of electromagnetic waves, good electrical and magnetic properties such as hematite (Fe_3O_4) [10,11]. Low-cost material, safe and it has a similar function with Pb in the protection radiation. Therefore, the combination of the Fe and carbon materials must be continue to study to find the maximum composition with the best characteristics for protecting the radiation dose transmit to the medical workers [9].

The effectiveness of materials in the protection of radiation in the form of the apron can be seen by the density, attenuation coefficient (μ), mass attenuation coefficient (μs), half-value layer (HVL), and mean free path (MFP) [9,12–14]. To the best of our knowledge there is no reported of these properties for composite cassava starch/BC/Fe_3O_4/glycerin. In this research apron synthesized in the form of composite cassava starch/BC/Fe_3O_4/glycerin by varying the amount of Fe_3O_4 to find the maximum composition for the best characteristics in supporting the absorption properties [15,16].

The effect of amount of Fe_3O_4 in composite cassava starch/BC/Fe_3O_4/glycerin to the optical and absorption properties as the fundamental knowledge to understand the mechanism and the relation between these properties in supporting the performance of composite which has not experimentally investigated adequately. In this study, the

* Corresponding author.
E-mail address: dtahir@fmipa.unhas.ac.id (D. Tahir).

https://doi.org/10.1016/j.optmat.2021.110887
Received 31 December 2020; Accepted 1 February 2021

quantitative analysis of the FTIR spectra used to determine the optical properties in the form of the refractive index (n) and extinction coefficient (k) and then continue to find the dielectric function (ε), energy loss function (ELF) (Im $(-1/\varepsilon)$), attenuation constant, and propagation constant. From an analysis of the optical properties, the longitudinal (LO) and transversal (TO) optical phonon vibration identified. The effect of amount of Fe_3O_4 in composite cassava starch/BC/Fe_3O_4/glycerin to the optical properties and Gamma ray absorption properties is used to find the best characteristic in supporting material performance.

2. Experiment

2.1. Materials

Glycerin ($C_3H_8O_3$) (Merck) (molecular weight 92.09, boiling point 290°C), aquades, Fe_3O_4 was purchased from sigma aldric, black carbon (BC) from PT Cahaya Indo Abadi Indonesia, and cassava starch from local brand (Rose Brand Indonesia).

2.2. Sample Preparation

Fe_3O_4 in this study was varied 0.5%, 1%, and 1.5% (from the total amount of composite) mixed with black carbon (1%) using a Retsch mixing machine type MM400 (the year 2011, serial number: 121101082213) for 30 min to get composite Fe_3O_4–BC. After that, Fe_3O_4–BC was mixed with 10 g cassava starch, 6 g of glycerin, and 94 mL of aquades by stirring in a constant speed 900 rpm at 160 °C until the solution becomes a gel. The apron solution then poured into a mold (10 cm × 10 cm x 2 cm) and then heated by using a furnace at 70 °C for 12 h. The synthesis process of geopolymer apron can be seen clearly in Fig. 1.

2.3. Characterization

Bioplastic.

XRF is used to determine the composition of elements or compound of materials [17] in the form of solids, powder, and liquid. X-ray method were performed using a thermo ARL QUANT'S EDXRF model. The EDXRF spectrometer is equipped with an X-Ray tube cooler (Rh anode, 50 W maximum power), a cooling device, a drifted crystal detector, and a pulse processor (32 bits).

Fourier Transforms Infrared (FTIR) spectroscopy (Shimadzu Corp) type IRPrestige-21 spectrometers with triglycine sulfate doped with L-alanine (DLATGS) detectors, bright ceramic light sources, and KBr beam splitters. FTIR identifying functional groups and chemical bonds in the form of vibration modes of the covalent bonds at wavenumber in the range 4000–400 cm^{-1} of its transmittance without damage the sample [9,18,19].

Gamma-ray absorption is measured by the radiation dose using IBT 103 Irradiator radiation source from the Cesium (Cs)-137 isotope at the Health Facilities Maintenance Agency (BPFK) Makassar, Indonesia. The schematic illustration of the irradiator with the energy of 662 keV as shown in Fig. 2 for measuring the intensity of gamma radiation passing through the composites for the various compositions of Fe_3O_4. The sample is placed in the hole of IBT 103 irradiator then gamma rays will be transmitted to the pendosimeter. The measured intensity will be recorded on the pendosimeter in units of μSv. For the additional, the mechanical strength of the composite in the form of a tensile strength also discussed.

3. Data analysis

The FTIR spectra was recorded in the percent of transmittance (T%) between the light intensity transmitted through the samples (I) to the incident light intensity (I_0). The spectra need to be convert to the reflection (R(ω)) using the following equations [20–22]:

$$A(\omega) = 2 - \log[T(\omega)\%] \tag{1}$$

$$R(\omega) = 100 - [T(\omega) + A(w)] \tag{2}$$

The reflection (R(ω)) is used as input parameter to the phase change $\phi(\omega)$:

$$\phi(\omega) = -\frac{\omega}{\pi}\int_0^{\infty} \frac{lnR(w') - lnR(\omega)}{\omega'^2 - \omega^2} \tag{3}$$

For the simple computations, we applied the K–K relation in (3), form new equation:

$$\phi(\omega_j) = -\frac{4\omega_j}{\pi} x\, \omega\, x \sum_i \frac{\ln\left(\sqrt{R(\omega)}\right)}{\omega_i^2 - \omega_j^2} \tag{4}$$

where, j is a series of wavenumber. If j is an odd number, i is 2,4,6,8,...,j-1, and j+1, and when j is an even number, i is 1,3,5,7,...,j-1,j+1,... $\Delta\omega = \omega_{i+1} - \omega_i$. equation (4) was the input parameter for determining the

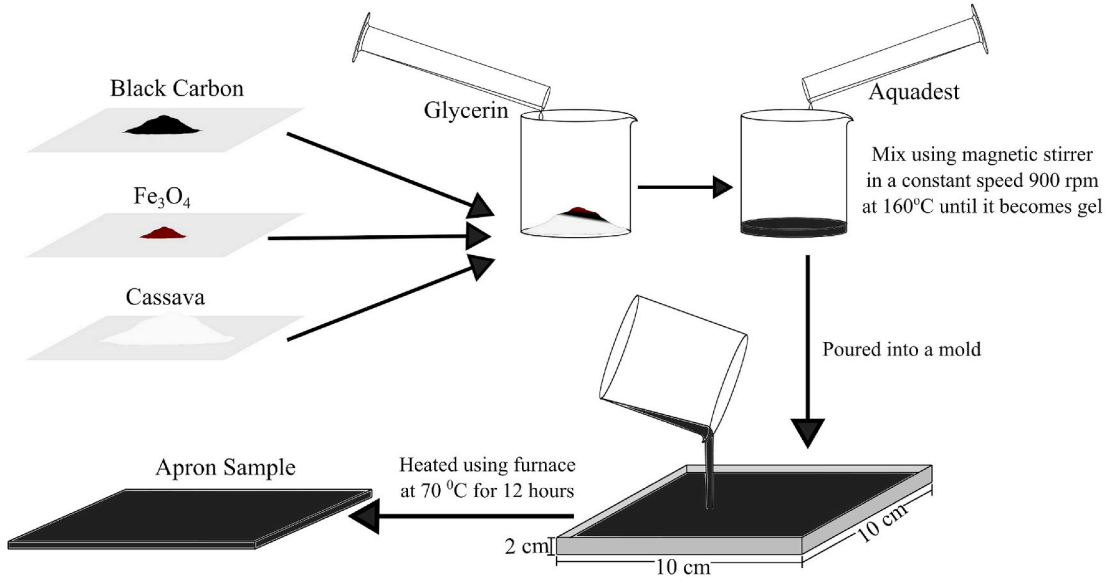

Fig. 1. Schematic illustration for the synthesis process composite apron in this study with various amount of Fe_3O_4.

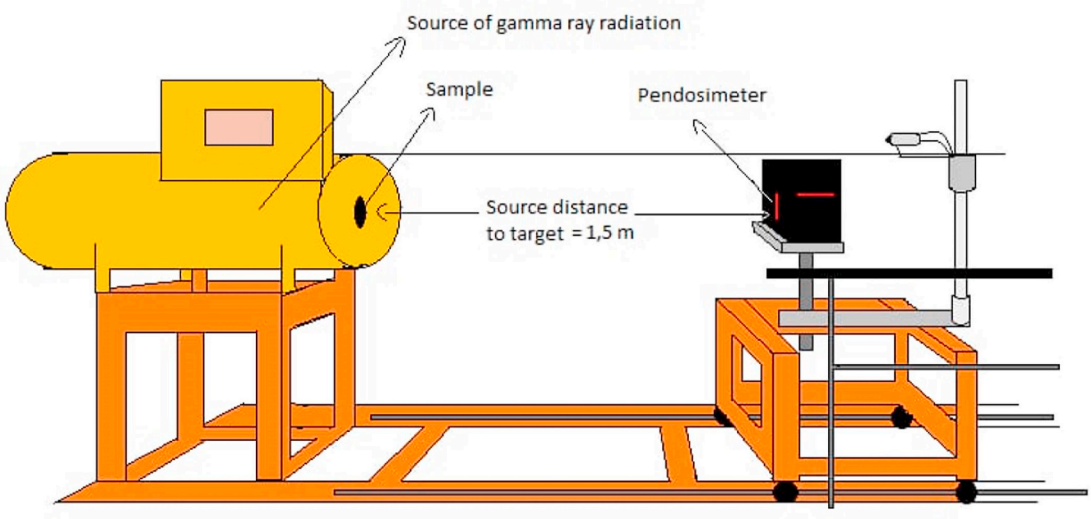

Fig. 2. Schematic illustration irradiator IBT 103 at the health facilities maintenance agency (BPFK) Makassar Indonesia.

refractive index (n) and extinction coefficient (k) by the following relations:

$$n(\omega) = \frac{1 - R(\omega)}{1 + R(\omega) - 2\sqrt{R(\omega)}\cos\phi(\omega)} \tag{5}$$

$$k(\omega) = \frac{2\sqrt{R(\omega)}sin\phi(\omega)}{1 + R(\omega) - 2\sqrt{R(\omega)}\cos\phi(\omega)} \tag{6}$$

The complex dielectric function in the form of $(\tilde{\varepsilon}(\omega) = \varepsilon_1(\omega) + i\varepsilon_2(\omega))$, where $\varepsilon_1(\omega)$ is the real part and $\varepsilon_2(\omega)$ is the imaginary part determined as follows:

$$\varepsilon_1(\omega) = n^2(\omega) - k^2(\omega) \tag{7}$$

$$\varepsilon_2(\omega) = 2n(\omega)k(\omega) \tag{8}$$

From the dielectric function, the energy loss function (ELF) $\left(Im\left(\frac{-1}{\varepsilon(\omega)}\right)\right)$, the attenuation constant α, and propagation constant β can be determined by the following relations:

$$Im\left(\frac{-1}{\varepsilon(\omega)}\right) = \left(\frac{\varepsilon_1(\omega)}{(\varepsilon_1^2(\omega)) + (\varepsilon_2^2(\omega))}\right) \tag{9}$$

$$\alpha = \omega\sqrt{\frac{\mu_0\varepsilon_0\varepsilon_{1(\omega)}}{2}\left[\sqrt{1 + \left(\frac{\varepsilon_2(\omega)}{\varepsilon_1(\omega)}\right)^2} - 1\right]} \tag{10}$$

$$\beta = \omega\sqrt{\frac{\mu_0\varepsilon_0\varepsilon_{1(\omega)}}{2}\left[\sqrt{1 + \left(\frac{\varepsilon_2(\omega)}{\varepsilon_1(\omega)}\right)^2} + 1\right]} \tag{11}$$

where μ_0 is permeability and the ε_0 is permittivity in a free space.

The mass density of the sample was calculated using:

$$\rho = \frac{m}{V} \tag{12}$$

where ρ is the mass density (g/cm^3), m is the mass (g), and V is the volume of the sample. The attenuation coefficient (μ) determined by the following equation with I_0 is initial radiation intensity and the I is radiation intensity through the sample.

$$\mathrm{I} = I_0 e^{-\mu d} \tag{13}$$

where μ is the attenuation coefficient (cm^{-1}) and d is the thickness of the sample (cm). While the mass attenuation coefficient is calculated by the following equation:

$$\mu_s = \frac{\mu}{\rho} \tag{14}$$

Where μ_s is mass attenuation coefficient (cm^2/g), μ is linear attenuation coefficient (cm^{-1}), and ρ is the mass density (g/cm^3). HVL is determined from the thickness of the radiation shielding which produces half of the initial intensity. The HVL value can be calculated by:

$$\mathrm{HVL} = \frac{0.693}{\mu} \tag{15}$$

where HVL is the thickness of the sample which produces half of the initial intensity (I). The MFP is the average distance between two adjacent particle by the photons interactions (cm), calculated by:

$$\mathrm{MFP} = \frac{1}{\mu} \tag{16}$$

In the process of interaction between photon from the X-ray and the atoms of the shield, the photon loss their energy by three process; photoelectric effect, Compton scattering, and pair production. All these physical phenomena contributed to the absorption of an apron materials which determined by the following equation:

$$\mathrm{DS} = \left(1 - \mathrm{e}^{-\mu d}\right) \text{ x } 100\% \tag{17}$$

where DS is absorption (%) and d is the thickness (cm).

4. Result and discussion

Cassava starch with Fe_3O_4 can be used apron by improving the electrical and mechanical properties of the polymer by mixture with carbon black [2]. For composite without Fe_3O_4 (Fe_2O_3–FeO) shows exist 83.86% Fe_2O_3 in composite which probably come from carbon black and cassava starch. For additional 0.5 g Fe_3O_4 shows Fe_2O_3 is 92.47% in composite and increase up to 96.36% for 1.5 g Fe_3O_4 in composite as we expected, for detail XRF results shows in Table 1.

Fig. 3 shows FTIR spectra for determining the functional groups by the additional of Fe_3O_4. Fig. 3 (a) shows for composite without Fe_3O_4 and an additional Fe_3O_4 in composite for (b), (c), and (d). The bonding formation in the composites are O–H, Si–O, C = O, C–N, C–O, and Fe–O, the corresponding wavenumbers are shown in Table 2.

At the wavenumbers 560 cm^{-1} is assigned Fe–O, at 1020 cm^{-1} for

Table 1
Chemical oxide composition composite apron from the X-ray fluorescence (XRF) for various composition of F_3O_4 in this study. We have included the composite apron without Fe_3O_4 (APFE0.0 (%)) as a control.

Oxide Compounds	APFE0.0 (%)	APFE0.5 (%)	APFE1.0 (%)	APFE1.5 (%)
SiO_2	8.41	5.65	2.82	2.59
CaO	6.98	1.07	0.715	0.58
Fe_2O_3	83.86	92.47	95.84	96.36
MnO	0.75	0.81	0.62	0.47

C–O, and at 1060 cm^{-1} for C–N bond. Asymmetrical and symmetrical stretching of C═O was observed from the wavenumber 1631 to 1645 cm^{-1} and the stretching vibration of the C–O bond at the wavenumber 1019-1024 cm^{-1} [17,23]. At wavenumbers 2000-2500 cm^{-1} assigned for Si–O bond [9]. The fourth area, which is in the range of the wavenumbers 3000-3500 cm^{-1} for the absorption of the O–H and C–H aldehyde groups [18,24,25]. The addition of Fe_3O_4 shows shifted to the lower wavenumbers of C–O and C═O, may due to the local bond asymmetry and weak of the bonds among them as the effect of the bonding nature of C atoms in composite is dominant metallic and covalent but also little ionic character. Another possibility may the Fe atoms doesn't sit in properly in the lattice structure that may effect of local strain and bond asymmetry produced bonding C-O_x-Fe_{1-x}. Strong and sharp absorption at the wavenumbers 1160 cm^{-1} from C–N group. From the XRF shows the composition of iron in the composite apron for gamma ray radiation becomes the majority and from the FTIR indicated that almost all primary bonding will bond with Fe, ex. for Si-O_x-Fe_{1-x} and C-O_x-Fe_{1-x}.

The optical properties as shown in Fig. 4 were determined from the quantitative analysis of FTIR spectra from Fig. 3. The first rows of Fig. 4 show refractive index (n) and extinction coefficient (k) as a function of the wavenumber. The intersection between n and k assigned as LO for longitudinal optical and TO for transversal optical phonon mode [25,26], and the distance between two optical phonon modes ((LO-TO)) is shown in Table 3. The stable bonding with a new structure [19,27] between filler (Fe_3O_4 and carbon black) and matrix shows 1.5% Fe_3O_4 in the composite, indicated by the ((LO-TO)) is higher.

The main peak of the imaginary part (ε_2 (ω)) of the dielectric function in Fig. 4 (second rows) uses for conform the TO vibration mode position and shows high consistency, similar for LO modes confirmed from the energy loss function (ELF) (Im $(-1/\varepsilon_1(\omega))$ in the third rows of Fig. 4. The TO and LO wavenumber position for composite shows increase with increasing the amount of Fe_3O_4 in the composite from 0.5% to 1.5%, indicated going more stable bonding in the lattice structure [26]. For composite apron without Fe_3O_4, the LO and TO is high may due the stable bonding connection between carbon atom with cassava starch and glycerin [28]. The ELF was identified as a plasma frequency

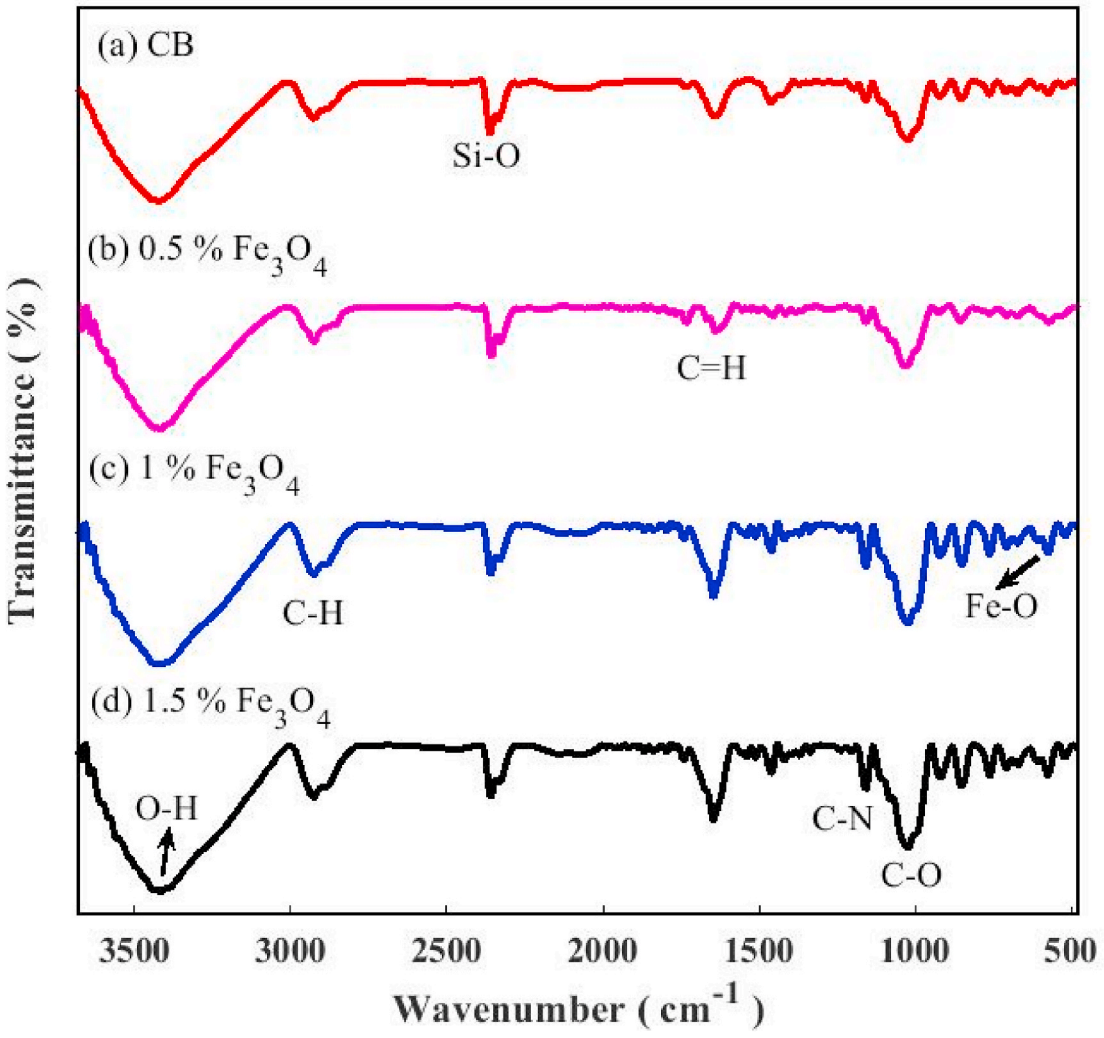

Fig. 3. Fourier transform infrared (FTIR) spectra of the composite apron as a function of concentration of Fe_3O_4. We have included the composite apron without Fe_3O_4 (CB) as a control.

Table 2
Wavenumber position for the corresponding chemical bond from the Fourier transform infrared (FTIR) spectra with various amount of Fe_3O_4 in composite apron.

Wavenumber (cm^{-1})				Chemical
APFE0.0	APFE0.5	APFE1.0	APFE1.5	Bond
3424	3431	3417	3405	O–H
2926	2912	2926	2926	C–H
2360	2353	2353	2353	Si–O
1645	1631	1645	1638	C=O
1160	1154	1140	1160	C–N
1024	1019	1025	1012	C–O
0	564	577	571	Fe–O

[28]. The ELF from the quantitative analysis of FTIR spectra was reported for composite cement/$BaSO_4$/Fe_3O_4 [25], for composite Fe/CNs/PVA [29], and composite geopolymer fly ash-metal [28].

The attenuation constant (α) and the propagation constant (β) shows in Fig. 5 using dielectric function in Fig. 4 as the input parameters in the calculation. The attenuation constant shows increase with increasing the amount of Fe_3O_4 in composite from 91.244 for 0.5% Fe_3O_4, 101.275 for 1% Fe_3O_4, and 455.688 for 1.5% Fe_3O_4, similar trend for propagation constant. It is indicated that the best composite in attenuating and easily propagating between the atoms of the electromagnetic wave for composite 1.5% Fe_3O_4 [30]. For composite apron without Fe_3O_4 in composite shows higher than the low amount of Fe_3O_4 in composite may due to the effect stable cross linking bond between carbon atom and cassava starch–glycerin atoms [28].

Table 3 shows density of each sample, mass attenuation coefficient, and the thickness, from Table 2, shows clearly the highest density is

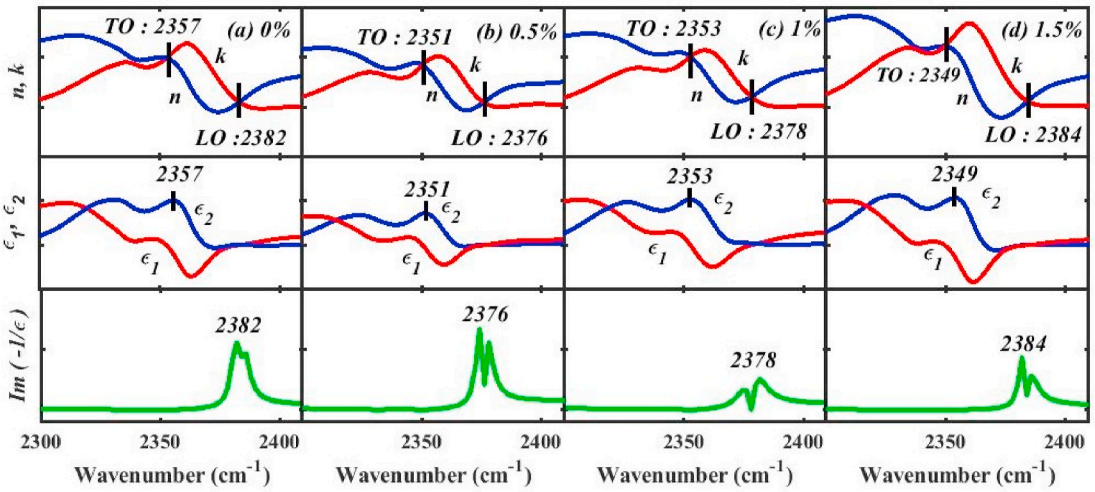

Fig. 4. The refractive index (n) and the extinction coefficient (k) (top row), the real part (ε_1) and imaginary part (ε_2) of dielectric function (middle row), and the energy loss function Im ($-1/\varepsilon_1(\omega)$) (bottom row) derived from the quantitative analysis of FTIR spectra in Fig. 3 for composite apron in this study as a function of concentration Fe_3O_4 from 0% (a) to 1.5% (d). The optical phonon vibration mode assigned by TO for transversal optical and LO for longitudinal optical (first rows).

Table 3
Attenuation coefficient for the energy 662 KeV, density, thickness, the distance between two optical vibration mode (Δ(LO-TO)) from Fig. 4, attenuation constant, and propagation constant from Fig. 5 for composite determined in this study.

Sample	Density (g/cm^3)	Thickness (cm)	Attenuation coefficient (cm^{-1})	Mass attenuation coefficient	Δ(LO-TO)	Att. Constant	Prop.
					cm^{-1}		constant
APFE0.0	0.846	0.114	0.147	0.201	25	141.035	709.556
APFE0.5	0.846	0.114	0.147	0.201	25	91.244	616.253
APFE1.0	0.980	0.115	0.166	0.169	25	101.275	747.767
APFE1.5	0.984	0.115	0.178	0.181	35	455.688	1255.00

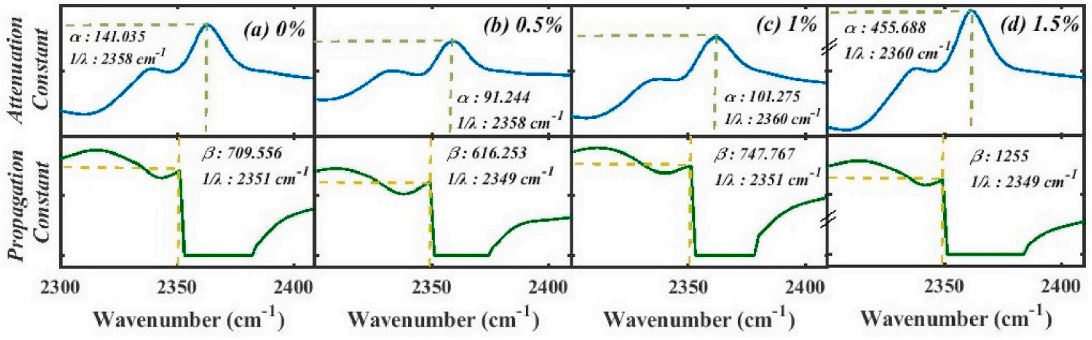

Fig. 5. The attenuation constant (α) (top rows) and the propagation constant (β) (second rows) for composite apron in this study as a function of concentration Fe_3O_4 from 0% (a) to 1.5% (d).

APFE1. The highest attenuation coefficient shown by APFE1 is 0.178 cm^{-1} for energy 662 KeV. Ref. [17] reported bismuth based for radiation shield shows the linear attenuation coefficient is 0.240 cm^{-1}. The difference between Ref. [17] and results in study is 0.062 cm^{-1} probably due to the atomic mass between iron and bismuth are different, the atomic mass of iron is 55,845 u while bismuth is 208,9804 u [23,31]. A good radiation shield has a large density more effective for absorbing gamma radiation, the corresponding calculation results presented in Table 3. Ref. [32] reported the radiation shield from PANi/Pb material with the thickness of 0.15 cm shows the attenuation coefficient is 0.909 cm^{-1} for energy 60 keV comparing in this study by additional Fe_3O_4, the difference attenuation coefficient is 0.731 cm^{-1} but much higher irradiation energy of 662 keV.

The photoelectric absorption is highly dependent on the atomic number Z so that if the sample with a larger atomic number is much better to be used for radiation in the form of the apron [7,33,34]. Based on IEC 61331-1: 2002 [35] regarding for the apron standard of the world's best quality shows that, a thickness of 5 cm the apron can absorbing radiation of 0.9%. For the sample APFE1.5, can absorbing 0.1738% wave radiation for the thickness of 0.115 cm. By comparing to the international standards, the thickness in this study is 0.115 cm, must be able to absorb radiation at least 0.021% but we found that the absorption of 1.021%, indicated that high potentials of the composite apron in this study for gamma ray absorption.

The effectiveness of gamma-ray radiation absorption can be seen also from the attenuation coefficient and the mass attenuation coefficient. The higher of the both attenuation coefficient is indicated good to be used as a radiation retaining material. The highest values for attenuation coefficient, attenuation constant, propagation constant, and the distance between two optical phonon mode as shown in Table 3 is 1.5% Fe_3O_4 in composite, indicated that the Fe and O atoms successfully forming isotropic covalent bonding with atom C in the polymer matrix of composite apron [9]. HVL and MFP data in this study are shown in Fig. 6. HVL is the thickness of the material needed to reduce the intensity of X-rays by half from the initial intensity while the MFP is defined as the average distance between two interacting adjacent particles (cm) [9].

Based on Fig. 6, the best HVL is shown by APFE1.5 because it has a lower value compared to other geopolymer aprons. So, to reduce the intensity of the radiation to half the initial intensity, we need a absorber with a thickness of 4.175 cm. The best MFP in this study was demonstrated by APFE1.5 with a value of 5.618 cm.

Fig. 6 also shows the mechanical properties of the composite apron for an additional of carbon and various amount of Fe_3O_4 in composites. Tensile strength increases with increasing the amount of Fe_3O_4 in the composite. The best tensile strength shown by APFE1.5 is 54.700 MPa. The tensile test value is much better compared to the tensile test conducted by Ambika (2017) [36] whose value is 25 MPa for bismuth material. The higher value of the distance between two optical phonon vibration, attenuation constant, propagation constant was strong correlation with higher absorption properties and higher mechanical properties for composite in this study. The best these characteristic in supporting composite performance as an apron applications are by an additional 1.5% Fe3O4 in the composite.

5. Conclusion

Geopolymer apron cassava starch/BC/Fe_3O_4/glycerin has been successfully synthesized for Fe_3O_4 is 0.5%, 1%, and 1.5% by simple methods. The stable bonding between filler (Fe_3O_4 and carbon black) and matrix with a new structure shows for composite 1.5% Fe_3O_4 as confirmed by the ((LO-TO)) is higher. The highest values for attenuation coefficient, attenuation constant, propagation constant, and the distance between two optical phonon mode ((LO-TO)) is composite 1.5% Fe_3O_4, indicated that the Fe and O atoms successfully forming isotropic covalent bonding with atom C in the polymer matrix. The best characteristic in supporting composite performance as an apron applications are for 1.5% Fe_3O_4 in the composite. The attenuation was 0.178 cm^{-1}, sample density was 0.984 g/cm^3, HVL value was 3.893 cm, and MPF was 5.618

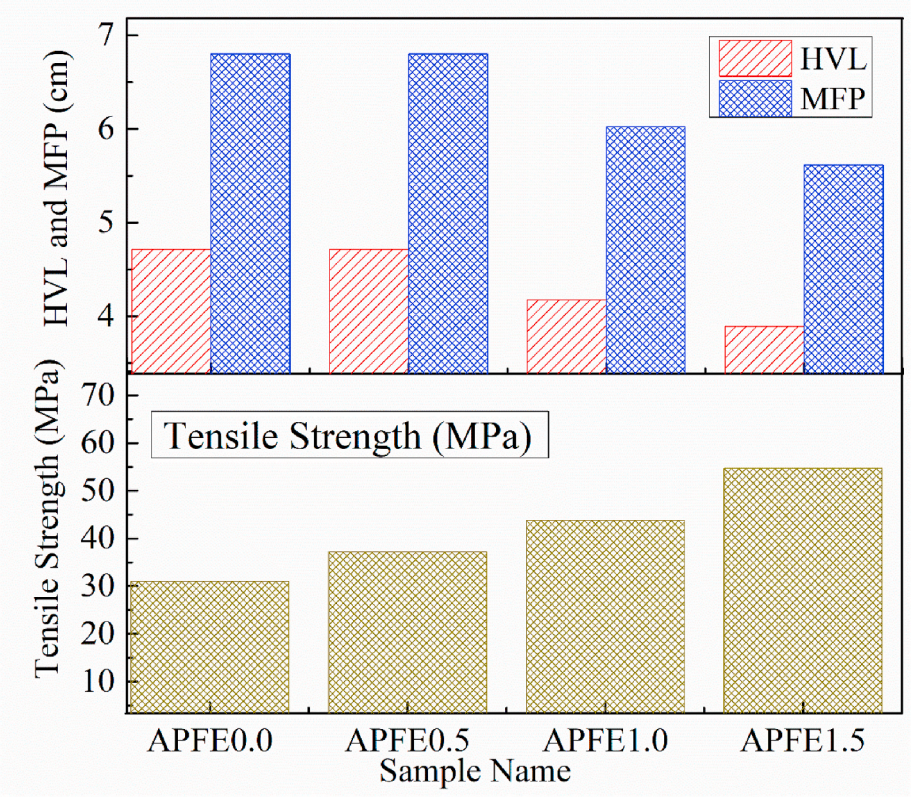

Fig. 6. The HVL and MFP (top rows) and the Tensile strength (second rows) for composite apron in this study as a function of concentration Fe_3O_4 from 0% to 1.5%.

cm. This study shows that the infrared spectroscopy is efficient methods for determining the optical properties, phonon vibration, dielectric function, energy loss function, attenuation constant, and propagation constant of composite apron cassava starch/BC/Fe_3O_4/glycerin.

Declaration of competing interest

The authors declare that they have no known competing financial interests or personal relationships that could have appeared to influence the work reported in this paper.

Acknowledgments

This work was supported by the PTM (Penelitian Tesis Magsiter) funded by the Indonesia Government (Kemenristek/BRIN) grants: 1517/UN4.22/PT.01.03//2020.

References

[1] N. Weber, P. Monnin, C. Elandoy, S. Ding, A model-based approach of scatter dose contributions and efficiency of apron shielding for radiation protection in CT, Phys. Med. 31 (2015) 889–896.
[2] G.S. Lohar, B.F. Jogi, Influence of carbon black (CB) on mechanical behaviour and microscopic analysis of poly-propylena (PP) acrylonitrile-butadine-styrene (ABS) nanocomposites, Procedia Manuf. 20 (2018) 85–90.
[3] S. Chhetri, N.C. Adak, P. Samanta, M.C. Naresh, S.K. Srivastava, T. Kuila, Synergistic effect of Fe_3O_4 anchored N-doped rGO hybrid on mechanical, thermal and electromagnetic shielding properties of epoxy composites, Compos. B Eng. 166 (2019) 371–381.
[4] E. Horszczaruk, P. Brzozowski, Investigation of gamma ray shielding efficiency and physicomechanical performances of heavyweight concrete subjected to high temperature, Construct. Build. Mater. 195 (2019) 574–582.
[5] R. Biswas, H. Sahadath, A.S. Mollah, Md.F. Huq, Calculation of gamma-ray attenuation parameters for locally developed shielding material: polyboron, J. Rad. Res. Appl. Sci. 9 (2016) 26–34.
[6] A.M. Madbouly, E.R. Atta, Comparative study between lead oxide and lead nitrate polymer as gamma-radiation shielding materials, J. Environ. Protect. 7 (2) (2016) 268–276.
[7] S.J. Hyun, K.J. Kim, T.A. Jahng, H.J. Kim, Efficiency of lead aprons in blocking radiation – how protective are they? Heliyon 2 (2016), e00117, 1-14.
[8] M. Dogra, K.J. Singh, K. Kaur, V. Anand, P. Kaur, Gamma ray shielding and structural properties of Bi_2O_3-B_2O_3-Na_2WO_4 glass syste, Univ. J. Phys. Appl. 11 (5) (2017) 190–195.
[9] Nurhasmi, D. Tahir, B. Abdullah, A. Ansar, S. Ilyas, I. Mutmainna, W.I. Madda, Geopolimer concrete for radiation shielding application, Mater. Sci. Forum 966 (2019) 41–47.
[10] H.O. Tekin, M.I. Sayyed, S.A.M. Issa, Gamma radiation shielding properties of the hematite-serpentine concrete blended with WO_3 and Bi_2O_3 micro and nano particles using MCNPX code, Radiat. Phys. Chem. 150 (2018) 95–100.
[11] M.A. Budiawan, S. Suryani, B. Abdullah, D. Tahir, Analysis of absorption properties of a composite FlyAsh and Fe_2O_3 for X-ray radiation shielding applications, IOP Conf. Ser. Mater. Sci. Eng. 593 (2019) 1–4.
[12] N. Chanthima, J. Kaewkhao, P. Limkitjaroenporn, S. Tuscharoen, S. Kothan, M. Tungjai, S. Kaewjaeng, S. Sarachai, P. Limsuwan, Development of BaO-ZnO-B_2O_3 glasses as A radiation shielding material, Rad. Phys. Chem. 137 (2016) 72–77.
[13] R.S. Kaundal, Comparative study of radiation shielding parameters for bismuth borate glasses, Mater. Res. 19 (4) (2016) 776–780.
[14] D.K. Gaikwad, M.I. Sayyed, S.S. Obaid, S.A.M. Issa, P.P. Pawar, Gamma ray shielding properties of TeO_2-ZnF2-as_2O_3-Sm_2O_3 glasses, J. Alloys Compd. 765 (2017) 451–458.
[15] Y. Zhan, Z. Long, X. Wan, J. Zhang, S. He, Y. He, 3D carbon fiber mats/nano-Fe_3O_4 hybrid material with high electromagnetic shielding performance, Appl. Surf. Sci. 444 (2018) 710–720.
[16] B. Abdullah, S. Ilyas, D. Tahir, Nanocomposites Fe/activated carbon/PVA for microwave absorber: synthesis and characterization, J. Nanomater. (2018) 1–6.
[17] B. Abdullah, Annisyah, S. Ilyas, D. Tahir, Structural properties and bonding characteristics of honeycomb structure of composite $ZnMnO_2$ and activated carbon, J. Appl. Biomater. Funct. Mater. 17 (2019) 1–6.
[18] Y.K. Lahsmin, D. Tahir, B. Abdullah, S. Ilyas, I. Mutmainna, Synthesis of carbon nanosphere at low temperatures based on bamboo fiber, Mater. Sci. Forum 966 (2019) 163–168.
[19] S. Ilyas, B. Abdullah, D. Tahir, Enchanment of adsorbing frequency and photo-catalytic performance by temperature treatment of composites Fe_3O_4-AC nanoparticle, Adv. Powder Technol. 31 (3) (2020) 905–913.
[20] Gh H. Khorami, A.K. Zak, A. Kompany, R. yousefi, Optical and structural properties of X-doped (X = Mn, Mg, and Zn) PZT nanoparticles by Kramers–Kronig and size strain plot methods, Ceram. Int. 38 (2012) 5683–5690.
[21] Y. Li, W. Qiu, F. Qin, H. Fang, V.G. Hadjiev, D. Litvinov, J. Bao, Identification of cobalt oxides with Raman scattering and fourier transform infrared spectroscopy, J. Phys. Chem. C 120 (2016) 4511–4516.
[22] B. Kanyathare, B. Asamoah, K.E. Peiponen, Imaginary optical constants in nearinfrared (NIR) spectral range for the separation and discrimination of adulterated diesel oil binary mixtures, Opt. Rev. 26 (2019) 85–94.
[23] D. Tahir, S. Ilyas, B. Abdullah, B. Armynah, H.J. Kang, Electronic properties of composite iron (II, III) oxide (Fe_3O_4) carbonaceous absorber materials by electron spectroscopy, J. Electron. Spectrosc. Relat. Phenom. 229 (2018) 47–51.
[24] M.A. Anugrah, S. Suryani, S. Ilyas, I. Mutmainna, A.N. Fahri, Jusmawang, D. Tahir, Composite gelatin/Rhizophora SPP particleboards/PVA for soft tissue phantom application, Radiat. Phys. Chem. 173 (2020) 108878.
[25] S. Suryani, H. Heryanto, R. Rusdaeni, A.N. Fahri, D. Tahir, Quantitative analysis of diffraction and infrared spectra of composite cement/$BaSO_4$/Fe_3O_4 for determining correlation between attenuation coefficient, structural and optical properties, Ceram. Int. 46 (11) (2020) 18601–18607.
[26] S. Ilyas, H. Heryanto, D. Tahir, Correlation between structural and optical properties of CuO/carbon nanoparticle in supports the photocatalytic performance and attenuate the electromagnetic wave, J. Environ. Chem. Eng. 9 (1) (2021), 104670.
[27] X. Lu, J. Chen, M. Zheng, J. Guo, J. Qi, Y. Chen, S. Miao, B. Zheng, Effect of high-intensity ultrasound irradiation on the stability and structural features of coconut-grain milk composite systems utilizing maize kernels and starch with different amylose contents, Ultrason. Sonochem. 55 (2019) 135–148.
[28] Heryanto Nurhasmi, A.N. Fahri, S. Ilyas, A. Ansar, B. Abdullah, D. Tahir, Study on optical phonon vibration and gamma ray shielding properties of composite geopolymer fly ash-metal, Radiat. Phys. Chem. 180 (2021) 109250.
[29] Y.K. Lashmin, H. Heryanto, S. Ilyas, A.N. Fahri, B. Abdullah, D. Tahir, Optical properties determined from infrared spectroscopy and structural properties from diffraction spectroscopy of composites Fe/CNs/PVA for electromagnetic wave absorption, Opt. Mater. 111 (2021), 110639.
[30] H. Cai, B. Cheng, H. Xiao, Q. Wei, Synthesis of rGO/p-Fe_3O_4@PANI three-phase nanomaterials and electromagnetic wave absorption properties, Mater. Res. Express 6 (2019) 125621.
[31] D. Tahir, S. Ilyas, B. Abdullah, B. Armynah, K. Kim, H.J. Kang, Modification in electronic, structural, and magnetic properties based on compositttion of composites copper (II) oxide (CuO) and carbonaceous Material, Mater. Res Express 6 (2019), 035705.
[32] S.H. Hosseini, M. Askari, S.N. Ezzati, X-ray attenuating nanocomposite based on polyaniline using Pb nanoparticles, Synth. Met. 196 (2014) 68–75.
[33] H. Cheng, S. Wei, Y. Ji, J. Zhai, X. Zhang, J. Chen, C. Shen, Synergetic effect of Fe_3O_4 nanoparticles and carbon on flexible poly (vinylidence fluoride) based films with higher heat dissipation to improve electromagnetic shielding, Compos. Appl. Sci. Manuf. 121 (2019) 139–148.
[34] M.I. Sayyed, S.A.M. Issa, H.O. Tekin, Y.B. Saddeek, Comparative study of gamma-ray shielding and elastic properties of BaO–Bi_2O_3–B_2O_3 and ZnO–Bi_2O_3–B_2O_3 glass systems, Mater. Chem. Phys. 217 (2018) 11–22.
[35] IEC 61331-1: 2002 international radiation protection, Mater. Stand. 11 (2017). Update June.
[36] M.R. Ambika, N. Nagaiah, V. Harish, N.K. Lokanath, M.A. Sridhar, N. M. Renukappa, S.K. Suman, Preparation and characterisation of ishophthalic Bi_2O_3 polymer composite gamma radiation shields, Radiat. Phys. Chem. 130 (2016) 352–358.